Journal of Materials Chemistry B

ROYAL SOCIETY OF CHEMISTRY

PAPER

View Article Online
View Journal | View Issue

Cite this: J. Mater. Chem. B, 2025, 13, 3716

A biomimetic dual-targeting nanomedicine for pancreatic cancer therapy†

Guihua Zhou,[abc] Yuan Zhang,[e] Zhiwei Cai,[a] Hongfei Yao,[a] Meng Liu,[a] Chongyi Jiang*[a] and Zhen Cheng*[cd]

Received 1st October 2024,
Accepted 8th February 2025

DOI: 10.1039/d4tb02206h

rsc.li/materials-b

The physiological characteristics of pancreatic cancer (PC) involve the interplay between tumor cells, cancer-associated fibroblasts (CAF) and the extracellular matrix (ECM). This intricate microenvironment contributes to the cancer's resistance to conventional chemoradiotherapy and its poor prognosis. Carbon monoxide (CO), a promising molecule in gas therapy, can effectively penetrate solid tumors and induce tumor cell apoptosis at high concentrations. However, precise dosing control remains a significant challenge in the administration of exogenous CO, and its inherent toxicity at elevated concentrations presents substantial barriers to clinical translation. In this study, we developed a novel biomimetic nanomedical drug delivery system capable of simultaneously targeting CAF and PC tumor cells, degrading the ECM, and inhibiting tumor growth. The strategy integrates iron carbonyl (FeCO), an anti-cancer agent, and losartan (Lo), a drug that degrades tumor matrix, into a biodegradable nanomaterial—mesoporous polydopamine (MPDA). The resulting nanoparticles are then coated with CAF cell membranes (CAFM) and functionalized with plectin-1 targeted peptide (PTP), a molecule that targets PC cells, to construct the (Lo + FeCO)@MPDA@CAFM-PTP nanomedicine. This system utilizes the homologous adhesion properties of CAF membranes to target CAFs, delivering Lo to degrade the ECM. Following ECM degradation, the nanomedicine penetrates further to bind to PC tumor cells *via* PTP. Then anti-cancer drug FeCO is released to react with the excessive reactive oxygen species (ROS) in PC tumor cells to produce high concentrations of CO, effectively inducing tumor cell apoptosis. The (Lo + FeCO)@MPDA@CAFM-PTP nanomedicine demonstrated significant cytotoxicity against Panc-1 cells *in vitro* and effectively inhibited PC tumor growth *in vivo*. This innovative approach holds great promise for advancing pancreatic cancer treatment.

1. Introduction

Pancreatic cancer (PC) is one of the most lethal malignancies and ranks as the fourth leading cause of cancer-related deaths in Western countries.[1–4] Although surgery offers the only hope to cure this aggressive disease, only 10–20% of patients with PC are eligible for radical resection at the time of diagnosis.[1,5–8] Consequently, the primary treatment for PC relies on chemotherapy, which typically provides only limited benefits in most cases.[6,7] In recent years, gas therapy has been emerging as a promising therapeutic modality due to its "green" feature that is superior to traditional therapeutic drugs.[9,10] For cancer treatment, numerous studies have demonstrated that gaseous molecules such as carbon monoxide (CO), hydrogen sulfide (H_2S) and nitric oxide (NO) can selectively induce apoptosis in cancer cells without harming healthy tissues.[9–12] Among these gases, CO has attracted great interest in recent years because of its stability, as it does not react with intracellular metabolites and is less likely to be consumed in the body before reaching pathological sites.[13,14]

As is well known, CO is recognized as a toxic gas due to its ability to bind with hemoglobin (Hb), thereby reducing oxygen-carrying capacity and causing toxic effects.[10,11,15] However, an efficient delivery of CO to tumor tissue may mitigate its toxic effects and represents a promising approach for CO-based therapy.[11] Various CO-releasing molecules (CORMs) have been developed, which can be triggered by certain endogenous stimuli such as pH, hydrogen peroxide (H_2O_2), heat, or light

[a] Department of General Surgery, Huadong Hospital, Fudan University, Shanghai 200040, China. E-mail: jiangzhongyi9@126.com
[b] Department of Hepatobiliary Pancreatic Surgery, Changhai Hospital, Naval Medical University, Shanghai 200433, China
[c] State Key Laboratory of Drug Research, Molecular Imaging Center, Shanghai Institute of Materia Medica, Chinese Academy of Sciences, Shanghai 201203, China. E-mail: zcheng@simm.ac.cn
[d] Shandong Laboratory of Yantai Drug Discovery, Bohai Rim Advanced Research Institute for Drug Discovery, Yantai, Shandong 264117, China
[e] Department of General Surgery, Shanghai Ren-ai Hospital, Shanghai 200235, China

† Electronic supplementary information (ESI) available. See DOI: https://doi.org/10.1039/d4tb02206h

to release CO gas.[10,13] Triirondodecacarbonyl ($Fe_3(CO)_{12}$, abbreviated as FeCO) is a radical-sensitive metal carbonyl compound CORM that could be triggered by intratumoral overexpressed reactive oxygen species (ROS) to release CO and Fe^{2+} *via* a Fenton-like reaction.[9,12,16] It is well known that a solid tumor's microenvironment is not only hypoxic and acidic but also characterized by an overproduction of ROS, such as H_2O_2.[17,18] Similar to many other solid tumors, excessive accumulation of ROS is a hallmark of PC.[2,3,19,20] This characteristic could serve as a potential therapeutic avenue for utilizing FeCO in the treatment of solid tumors, such as PC.

Meanwhile, PC is markedly different from other cancers due to its extremely poor prognosis, which has driven the development of numerous drugs and treatment strategies, such as anti-angiogenic therapies and targeted drug delivery methods for tumor tissues.[1,21] But most clinical therapeutics focus primarily on cancer cells, often overlooking the tumor microenvironment (TME). The TME, which consists of abundant cancer-associated fibroblasts (CAFs) and excessive extracellular matrix (ECM), acts as a shielding physiological barrier, reducing the delivery of therapeutic drugs to tumor cells.[4,5,15,21–25] Therefore, addressing drug perfusion limitation by regulating or remodeling the TME may greatly improve the effect of PC treatment, and has attracted considerable research interest in recent years.[5,24,26] Recent studies have shown that the angiotensin inhibitor losartan (Lo), a widely prescribed antihypertensive drug, has antifibrotic ability that could reduce stromal component production and suppress profibrotic signaling in solid tumor models.[24,25] Through its antifibrotic effects, Lo can alleviate solid stress and decompress tumor vessels, thereby improving increased vascular perfusion and enhancing the delivery of drugs and oxygen.[24] Based on these findings, we hypothesize that combining Lo with FeCO in the treatment of PC might greatly enhance the efficacy of treatment. However, how to effectively deliver both drugs to the tumor site at the same time remains a challenge.

Nanoparticles can improve tumor tissue penetration and treatment efficacy, and this has been extensively explored.[1,6,11,27] Among these, mesoporous polydopamine (MPDA) stands out as a bioinspired nanoparticle that is polymerized by dopamine molecules spontaneously under alkaline conditions.[28–30] Compared to other nanoparticles, MPDA possesses several unique properties, including excellent biocompatibility and biodegradability, facile preparation, pH responsiveness, *etc*.[13,30–36] These attributes have garnered significant attention for MPDA in biomedical application research in recent years. Additionally, its porous structure and high drug-loading capacity have made it a promising candidate for smart drug delivery systems, prompting extensive investigation by researchers in recent years.[29,37,38] However, as exogenous materials, nanoparticles face several challenges, including early recognition by the immune system, fast clearance from blood circulation, and insufficient accumulation at tumor sites.[36,39] A biomimetic approach utilizing cell membrane coating to camouflage nanoparticles can enhance their biocompatibility. This strategy imparts nanoparticles with inherent properties and functions of cell membranes, improving their performance in biomedical applications.[26,27,36,39]

Plectin-1 is a cytolinker protein that is aberrantly expressed in all primary PC tumor cells, their metastatic deposits, and the majority of pre-invasive PanIN III lesions. Importantly, it is not expressed in benign tissues, making it a highly specific marker for distinguishing malignancy from benign conditions—an essential characteristic of an ideal PC biomarker.[7,40–42] The plectin-1 targeted peptide (PTP) specially binds to plectin-1. While the passive accumulation of most nanoparticles in lesion tissues relies heavily on the enhanced permeability and retention (EPR) effect, the targeting efficiency of EPR alone is relatively low. Conjugation with PTP enables nanoparticles to actively target PC cells, thereby enhancing their precision and effectiveness.[1,6,15,22,25–27,29,31,36]

In this study, we rationally designed a biomimetic multifunctional nanomedicine that can target both CAF cells and PC cells, degrade the stroma of TME, and release CO to kill or inhibit PC cells. First, we incorporated both FeCO and Lo into MPDA nanoparticles to obtain (Lo + FeCO)@MPDA nanoparticles. We then extracted CAF cell membrane (CAFM) nano nanovesicles and coated them on the surface of (Lo + FeCO)@MPDA nanoparticles to obtain (Lo + FeCO)@MPDA@CAFM nanoparticles. We then modified the surface of (Lo + FeCO)@MPDA@CAFM with the targeting molecule PTP to create the (Lo + FeCO)@MPDA@CAFM-PTP nanomedicine. In the treatment of PC tumors, we hypothesize that the (Lo + FeCO)@MPDA@CAFM-PTP nanomedicine will first target the CAF cells of the TME through homologous adhesion between CAFM and CAF cells. Following this, MPDA will degrade and release Lo, reducing the TME stroma and solid stress due to PC's acidic TME and MPDA's pH sensitivity. As the solid stress decreases, the solid PC tumor becomes looser, allowing more (Lo + FeCO)@MPDA@CAFM-PTP nanomedicine to diffuse deeper into the tissue and reach PC cells. The (Lo + FeCO)@MPDA@CAFM-PTP nanomedicine is then internalized by PC cells through the interaction between PTP and plectin-1, which is overexpressed on PC cells. In the acidic microenvironment of PC cells, FeCO is released and reacts with the intracellular overproduced ROS to release CO, ultimately killing PC tumor cells (Scheme 1). To our knowledge, this is the first report of a synergetic therapy that incorporates different drugs into a single nanoplatform capable of targeting multiple pathways for the treatment of PC.

2. Materials and methods

2.1. Materials

Pluronic F-127 was purchased from Innochem (China). Dopamine and losartan potassium were purchased from Macklin (China). Ammonia ($NH_3.H_2O$), methanol, ethanol, and acetone were obtained from Sinopharm (China). FeCO was purchased from Leyan (China). Hb was purchased from Shanghai yuanye Bio-Technology Co., Ltd (China). Sodium dithionite (SDT) was purchased from Anhui Senrise Technology Co., Ltd (China).

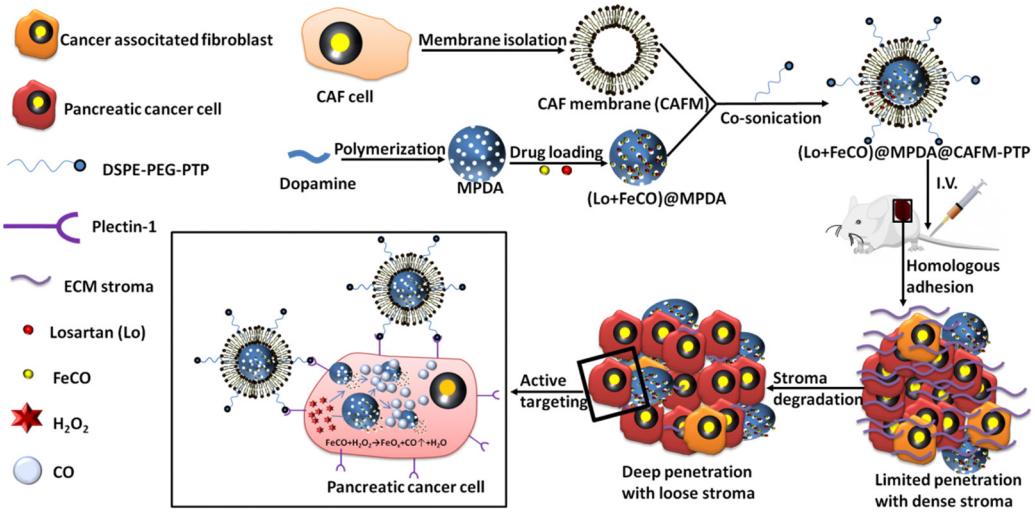

Scheme 1 Schematic illustration of the (Lo + FeCO)@MPDA@CAFM-PTP biomimetic dual-targeting nanomedicine preparation and its therapeutic effects on PC through targeting CAF and PC cells, extracellular matrix degradation, and CO gas therapy.

EDC was purchased from Energy Chemical (China). NHS was purchased from Bidepharm (China). PTP peptide was purchased from Tanshtech (China). DSPE-PEG-NH_2 was purchased from Ponsure Biological (China). Indocyanine green (ICG) was obtained from Shaanxi New Research Bioscience Co., Ltd (China). Panc-1, 3T3 and HUVEC cell lines were obtained from Meilun Biotechnology Co., Ltd (China). TGF-β1 was purchased from Peprotech (China). Plectin-1 antibody was bought from Santa Cruz Biotechnology, Inc. (Texas, USA). DCFH-DA was purchased from Dchem (China). CCK-8, matrix-gel and DAPI were bought from Beyotime (China).

2.2. Synthesis of mesoporous polydopamine (MPDA) nanoparticles

Typically, 1 g of F-127 and 0.5 g of dopamine were completely dissolved in 70 ml of ultra-pure water. To this solution, 0.5 mL of $NH_3{\cdot}H_2O$ was added, and the mixture was vigorously stirred for 24 h at room temperature to form MPDA nanoparticles. The MPDA nanoparticles were then collected by centrifugation at 12 000 rpm. To remove the template (F-127), the nanoparticles were washed several times with a mixture of ethanol/acetone mixture (v/v = 2 : 1).

2.3. Preparation of (Lo + FeCO)@MPDA nanoparticles

In this study, we employed a nano-casting method to fabricate (Lo + FeCO)@MPDA nanoparticles. This approach not only preserves the nanostructure and biocompatibility of MPDA, which facilitates cellular uptake and intracellular transport, but also enables a high drug loading capacity. First, Lo (5 mg), FeCO (5 mg), and MPDA nanoparticles (5mg) were completely dissolved in 30 mL of methanol. The solution was then degassed under vacuum in the dark until its volume was reduced to less than 1 mL. The final product was collected by centrifugation and washed twice with methanol. The supernatant and washing solutions were collected for measuring the drug loading capacity of MPDA for Lo and FeCO. The synthesised (Lo + FeCO)@MPDA nanoparticles were further washed twice with deionized water and then redispersed in 1 mL of PBS for further use.

The drug loading capacity of MPDA was determined using UV-vis spectroscopy. First, a series of FeCO methanol solutions with varying concentrations were prepared. The UV absorption of these solutions was then measured using a UV-vis spectrophotometer (Shimadzu UV-1800, Japan). A standard curve and linear correlation equation were established by analyzing the UV absorption data, relating solution concentration to absorption peak intensity. The same method was applied to determine the drug loading capacity of MPDA for Lo.

2.4. Synthesis of the DSPE-PEG-PTP conjugate

First, 1 mmol of PTP was completely dissolved in PBS solution (pH ~7.4), followed by the addition of 1.2 mmol of EDC and 0.8 mmol of NHS. The mixture was stirred at room temperature in the dark for 15 min to fully activate the carboxyl group (–COOH) of PTP. 0.9 mmol of DSPE-PEG-NH_2 was then added, and the solution was stirred at room temperature for 24 h to allow formation of the DSPE-PEG-PTP conjugate. The resulting product was purified by dialysis to remove unreacted compounds, using a dialysis bag with a molecular weight cutoff (MWCO) of 2.0 kDa. Dialysis was performed at least three times. Finally, the purified DSPE-PEG-PTP conjugate was dispersed in PBS solution and stored at 4 °C for further use.

2.5. Preparation of CAFM nanovesicles

3T3 fibroblasts were cultured in Dulbecco's modified Eagle's medium (DMEM) (hyclone) supplemented with 10% fetal bovine serum (FBS). TGF-β1 was then added to induce differentiation into CAF cells. To isolate CAFM nanovesicles, the CAF cells were collected and resuspended in 0.25× PBS solution overnight at 4 °C. The cell suspension was then subjected to 20 rounds of homogenization using a cell homogenizer. After homogenization, the suspension was centrifuged at 2000*g*

for 30 min at 4 °C. The supernatant, containing the CAF cell membranes, was collected and further centrifuged at 21 000*g*. After this second centrifugation, the supernatant was discarded, and the pellet containing the CAF cell membrane was retained. The resulting CAF cell membranes were resuspended in PBS and extruded through a Millipore membrane (pore size ~200 nm) using a mini extruder to produce CAFM nanovesicles. The extrusion process was repeated 20 times. The prepared CAFM nanovesicles were then dispersed in PBS and stored at 4 °C for further use.

2.6. Preparation of the (Lo + FeCO)@MPDA@CAFM-PTP nanomedicine

To prepare the (Lo + FeCO)@MPDA@CAFM-PTP nanomedicine, CAFM nanovesicles and DSPE-PEG-PTP were mixed with the (Lo + FeCO)@MPDA nanoparticles in an appropriate ratio. The mixed was then sonicated using an ultrasonic probe (JY88-IIN, SCIENTZ, China) for 2 min. Subsequently, the mixture was incubated on a shaker at 4 °C for 24 h, resulting in the formation of the (Lo + FeCO)@MPDA@CAFM-PTP nanomedicine. The (Lo + FeCO)@MPDA@CAFM nanoparticles were prepared using a similar method.

2.7. Verification of CO release from the (Lo + FeCO)@MPDA@CAFM-PTP nanomedicine

The conversion of Hb to carboxyhemoglobin (HbCO) was monitored using UV-vis spectrophotometry to confirm that the gas released during the reaction between (Lo + FeCO)@MPDA@CAFM-PTP and H_2O_2 was CO. First, Hb derived from bovine red blood cells was completely dissolved in a PBS solution containing H_2O_2. Next, the reducing agent SDT was added. The (Lo + FeCO)@MPDA@CAFM-PTP solution was bubbled with nitrogen gas to remove oxygen, and then introduced into the prepared Hb solution. The mixture was then immediately sealed in a UV quartz cuvette. UV absorption was measured using a UV-vis spectrophotometer (Shimadzu UV-1800, Japan). The HbCO absorption peak at 410 nm was used for qualitative analysis of HbCO production. The amount of CO released was quantified using the Lambert–Beer law.

2.8. Cell experiments

The fibroblast cell line 3T3 and PC cell line Panc-1 were used as the primary experimental cell models. The cells were cultured in DMEM (hyclone), supplemented with 10% FBS and 100 U mL^{-1} penicillin–streptomycin, at 37 °C in a 5% CO_2 incubator.

2.9. Cytotoxicity assay of nanoparticles

3T3 cells and panc-1 cells were seeded at 10 000 per well in 96-well plates. After 24 hours of incubation, a series of MPDA nanoparticles at varying concentrations were added to the medium, and the cells were co-incubated for additional 24 hours. Following incubation, the cells were washed with PBS three times, and cell viability was assessed using the CCK-8 assay. Additionally, the cytotoxicity of the (Lo + FeCO)@MPDA@CAFM-PTP nanomedicine was evaluated in vascular endothelial HUVEC cells using the same protocol to assess its biosafety in normal cells.

2.10. Transwell experiments

To more accurately simulate the physiological characteristics of PC as a solid tumor, cell experiments were conducted in Transwell chambers. 3T3 cells were seeded in the upper donor chamber and stimulated with TGF-β1 for 24 hours to mimic the ECM of PC. Panc-1 cells were then seeded in the lower acceptor chamber of the Transwell.

2.11. *In vitro* targeting effect of nanomedicine

ICG-labeled MPDA, (Lo + FeCO)@MPDA, (Lo + FeCO)@MPDA@CAFM, and (Lo + FeCO)@MPDA@CAFM-PTP nanoparticles (200 μg mL^{-1}, 20 μL) were added to donor chambers of a Transwell system. After incubation for 12 hours, Panc-1 cells in the acceptor chambers were washed with PBS, fixed with 4% paraformaldehyde, and stained with DAPI for 15 minutes. The cells were then washed with PBS 3 times and imaged under a fluorescence microscope to evaluate the targeting ability.

2.12. *In vitro* anti-cancer effect and intracellular ROS measurements

MPDA, (Lo + FeCO)@MPDA, (Lo + FeCO)@MPDA@CAFM, and (Lo + FeCO)@MPDA@CAFM-PTP nanoparticles (200 μg mL^{-1}, 20 μL) were introduced into the donor chambers of the Transwell system. A PBS-treated group was included as a control. After incubation for 12 hours, viability of Panc-1 cells in the acceptor chambers was detected *via* the CCK-8 assay to evaluate *in vitro* anti-cancer effects. In addition, we detected intracellular ROS of Panc-1 cells by DCFH-DA.

2.13. Animal experiments

All animal experiments were performed in accordance with the principles, policies and procedures set by the Chinese Academy of Sciences (CAS) for the care and use of laboratory animals. The approval number for these experiments is 2022-08-CZ-03.

The experimental subjects in this study were 6-week-old female nude mice, which were obtained from the Laboratory Animal Center at the Shanghai Institute of Materia Medica, CAS. The mice were individually numbered and allowed one week to acclimatize to their new environment before the experiment.

To better simulate the composition of PC as a solid tumor, a mixture of Panc-1 cells (2×10^6) and 3T3 cells (0.5×10^6) was subcutaneously injected into the right flank of each nude mouse to establish tumor models. Experiments were conducted once the tumor volume reached appropriate size. Tumor volume was calculated using the following formula: $V = (L \times W^2)/2$, where '*L*' and '*W*' represent the tumor length and width, respectively.

2.14. *In vivo* targeting experiments

When the tumor volume reached approximately 300 mm^3, we randomly divided the tumor-bearing nude mice into four groups (n = 3). The mice were then injected *via* the tail vein

with ICG-labeled MPDA, (Lo + FeCO)@MPDA, (Lo + FeCO)@MPDA@CAFM, and (Lo + FeCO)@MPDA@CAFM-PTP nanoparticles (200 μg mL^{-1}, 100 μL). *In vivo* imaging was performed using an IVIS fluorescence imaging system at designated time points (2, 6, 12 and 24 hours) post-injection.

Twenty-four hours after injection, the nude mice were euthanized for *ex vivo* imaging. The heart, liver, spleen, lungs, kidneys, and tumors were harvested and imaged using the IVIS imaging system. Subsequently, ICP-OES (ThermoICPOES7200, ThermoFisher, USA) was performed to quantify the iron content in the tumors and major organs.

2.15. *In vivo* anti-cancer experiments

Tumor-bearing nude mice were randomly divided into five groups (n = 5). Body weight and tumor volume were monitored and recorded every other day. Treatments began on day 13. The five groups of tumor-bearing mice were administered with PBS (control), MPDA, (Lo + FeCO)@MPDA, (Lo + FeCO)@MPDA@CAFM, and (Lo + FeCO)@MPDA@CAFM-PTP nanoparticles (200 μg mL^{-1}, 200 μL) *via* tail vain injection on days 13, 16, 19, and 22. On day 28, all mice were euthanized, and blood samples were collected for biochemical analysis. Major organs, including the heart, liver, spleen, lungs, kidneys, and tumors, were harvested for histopathological analysis. The organs and tumors were then subjected to hematoxylin and eosin (H&E) staining. Immunofluorescence staining was performed to assess the tumor matrix, ROS levels, and plectin-1 expression. TUNEL staining was used to evaluate cancer cell necrosis.

2.16. Statistical analysis

Data were presented as mean with standard deviation and analyzed using analysis of variance (ANOVA) to assess the statistical significance. A p-value of < 0.05 was considered statistically significant and expressed as an asterisk in the figures.

3. Results

3.1. Preparation and characterization of (Lo + FeCO)@MPDA@CAFM-PTP nanomedicine

MPDA nanoparticles were synthesized following previously reported procedures. The synthesis of MPDA is simple and cost-effective.[38,43] Under mildly alkaline conditions (pH ~8.5), dopamine undergoes self-polymerization in the presence of an organic template, forming PDA nanoparticles with a mesoporous structure. After the template is removed, MPDA nanoparticles are obtained.[13,17,36,44,45] Transmission electron microscopy (TEM) analysis revealed that the MPDA nanoparticles have a well-defined spherical morphology with a worm-like porous shell and exhibit a uniform particle size distribution (~110 nm) (Fig. 1a). FeCO and Lo were loaded into the MPDA nanoparticles using a nanocasting method to yield the (Lo + FeCO)@MPDA nanoparticles. No significant changes in the spherical morphology of the MPDA nanoparticles were observed after drug loading, but most of the mesoporous structures disappeared (Fig. 1b).

To isolate the cell membrane, we first stimulated fibroblasts (3T3 cells) with TGF-β1 to induce their transformation into CAF cells. The CAF cells were then lysed under hypotonic conditions to obtain the CAF cell membrane, which was extruded through 200 nm polycarbonate porous membranes to generate CAFM nanovesicles. The resulting CAFM nanovesicles were stained with PTAH and this was confirmed *via* TEM imaging (Fig. 1c).

The encapsulation of CAFM nanovesicles on the surface of (Lo + FeCO)@MPDA nanoparticles was achieved through co-sonication of CAFM and (Lo + FeCO)@MPDA. This was confirmed using scanning electron microscopy (SEM), suggesting that the mesoporous structure of the MPDA nanoparticles was completely lost and the surface became smooth after CAFM coating. The SEM analysis indicates that the CAFM coating was successful and that the (Lo + FeCO)@MPDA@CAFM nanoparticles were successfully formed (Fig. 1d). Additionally, we detected fibroblast activation protein-α (FAP-α), a transmembrane protein selectively expressed by CAFs rather than normal cells, on the surface of the (Lo + FeCO)@MPDA@CAFM nanoparticles. These results further confirm the successful coating of CAFM on the (Lo + FeCO)@MPDA@CAFM nanoparticles (Fig. S1, ESI†).

We then functionalized the membrane surface of (Lo + FeCO)@MPDA@CAFM nanoparticles with the PTP peptide using a lipid insertion method. First, the –COOH group of PTP peptide reacted with the amine (NH_2) group of DSPE-PEG-NH_2, resulting in the formation of a DSPE-PEG-PTP lipid–peptide conjugate (Fig. S2, ESI†). Subsequently, the lipophilic DSPE group of DSPE-PEG-PTP and the lipid bilayer structure of the cell membrane facilitated the insertion of the PTP peptide into the membrane surface of (Lo + FeCO)@MPDA@CAFM nanoparticles through physical attachment, forming the (Lo + FeCO)@MPDA@CAFM-PTP nanomedicine. This strategy was straightforward, simple, and did not compromise the structure or integrity of the cell membrane.[26]

Dynamic light scattering (DLS) analysis revealed that the particle size of (Lo + FeCO)@MPDA was 118 nm, while that of (Lo + FeCO)@MPDA@CAFM-PTP was 126 nm, both larger than MPDA (Fig. 1e). We also measured the polydispersity index (PDI) for each nanoparticle using DLS, and the results indicated a high-quality size distribution (Table S1, ESI†). The zeta potential was determined *via* electrophoretic light scattering (ELS), showing values of −24.87 mV for MPDA, −31.29 mV for (Lo + FeCO)@MPDA, and −35.79 mV after coating with the cell membrane to form the (Lo + FeCO)@MPDA@CAFM-PTP nanomedicine (Fig. 1f). These findings confirm the successful drug loading and CAF cell membrane coating.

The chemical element composition of the (Lo + FeCO)@MPDA@CAFM-PTP nanomedicine was analyzed using energy dispersive X-ray spectroscopy (EDS). The results showed a fairly homogeneous distribution of elements potassium (K), nitrogen (N), chlorine (Cl), and iron (Fe), indicating successful drug loading and confirming that the product was indeed (Lo + FeCO)@MPDA@CAFM-PTP nanomedicine (Fig. 1g).

To further investigate the chemical bond activity of the loaded FeCO and Lo, an FT-IR assay was performed. The results

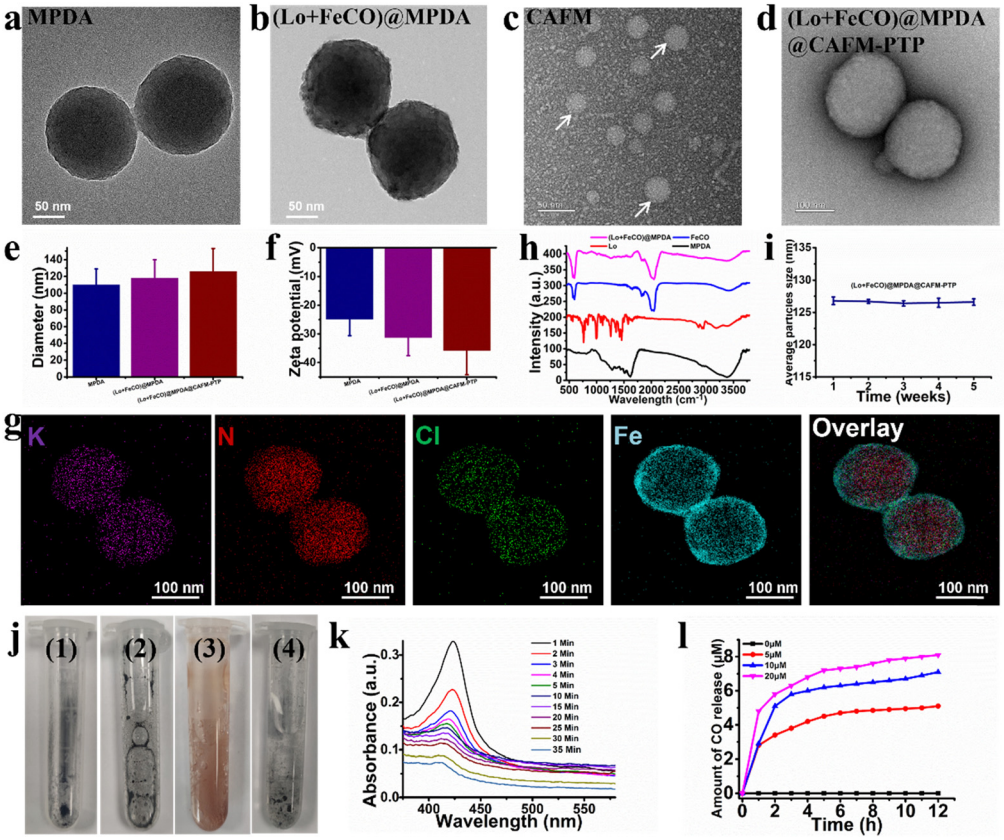

Fig. 1 Characterization of (Lo + FeCO)@MPDA@CAFM-PTP nanomedicine. TEM images of MPDA nanoparticles (a), (Lo + FeCO)@MPDA nanoparticles (b), CAF cell membrane nanovesicles (white arrows) (c), and SEM images of (Lo + FeCO)@MPDA@CAFM-PTP nanomedicine (d). The average particle size (e) and zeta potential (f) of MPDA, (Lo + FeCO)@MPDA, and (Lo + FeCO)@MPDA@CAFM-PTP nanomedicine. (g) Element mapping of (Lo + FeCO)@MPDA@CAFM-PTP nanomedicine for K, N, Cl, Fe, and their merged overlay image. (h) FT-IR spectra of Lo, FeCO, MPDA, and (Lo + FeCO)@MPDA@CAFM-PTP nanomedicine. (i) Change in particle size of (Lo + FeCO)@MPDA@CAFM-PTP nanomedicine store at 4 °C for 5 weeks. (j (1)) FeCO powder. (j (2–3)) Changes in FeCO in PBS with H_2O_2, where a significant amount of bubbles were generated, and the black FeCO powder gradually transformed into reddish-brown iron oxide (FeO_x) over time. (j (4)) No changes in FeCO in PBS without H_2O_2, even after 24 hours. (k) Changes in UV-vis absorption spectra of Hb during CO generation from (Lo + FeCO)@MPDA@CAFM-PTP nanomedicine in PBS with H_2O_2. (l) CO generation profile from (Lo + FeCO)@MPDA@CAFM-PTP nanomedicine in PBS with varying concentrations of H_2O_2.

demonstrated that both FeCO and Lo retained their chemical bond activity after being incorporated into the MPDA nanoparticles (Fig. 1h). X-ray photoelectron spectroscopy (XPS) analysis (Thermo Escalab 250Xi, USA) was conducted on the (Lo + FeCO)@MPDA@CAFM-PTP nanomedicine. The results were consistent with the EDS and FT-IR findings, further confirming the successful synthesis of the drug (Fig. S3, ESI†). The stability of (Lo + FeCO)@MPDA@CAFM-PTP nanomedicine was also assessed. The results showed no significant change in the average particle size after being stored in PBS for 5 weeks, indicating excellent stability (Fig. 1i).

The drug loading capacity was determined using a UV-vis method. Specifically, the UV-vis absorption intensity at 605 nm of a series of FeCO methanol solutions with different concentrations was measured (Fig. S4a, ESI†). Based on this, a standard curve and linear correlation equation between absorption intensity and FeCO concentration were established (Fig. S4b, ESI†). A similar approach was used to generate the standard curve and linear correlation equation between the UV-vis absorption intensity at 211 nm (Fig. S4c, ESI†) and the concentration of Lo methanol solution (Fig. S4d, ESI†). After the drug loading process, we measured the UV-vis absorption of the supernatant solution and calculated the drug loading capacity with the corresponding linear correlation equations. According to these equations, the drug loading capacity reached 496.875 mg of FeCO and 891.246 mg of Lo per gram of MPDA. This high drug loading capacity is very favourable for efficient cancer therapy.[11,29,31]

3.2. H_2O_2 triggers the release of CO from FeCO

To investigate the reaction mechanism of H_2O_2 triggering the release of CO from FeCO, freshly prepared FeCO was added to PBS, with or without H_2O_2, and reacted for 24h, respectively. In the presence of H_2O_2, numerous bubbles were generated, and the black FeCO gradually transformed into reddish-brown iron oxide (FeO_x) (Fig. 1j (1–3)). In contrast, no changes were observed in PBS without H_2O_2, even after 24 hours of reaction (Fig. 1j (4)).

We further used Hb as a probe to confirm the release of CO from (Lo + FeCO)@MPDA@CAFM-PTP upon stimulation by

H_2O_2, simulating the overproduction of ROS in cancer cells. CO can competitively bind to the heme group in Hb, forming HbCO, which induces a shift in the UV-vis absorption spectrum from 430 nm to 410 nm. In our experiment, we observed a clear shift of the UV-vis absorption peak of Hb to 410 nm in the presence of (Lo + FeCO)@MPDA@CAFM-PTP and H_2O_2, indicating CO generation (Fig. 1k). Furthermore, the amount of released CO increased with higher concentrations of H_2O_2, while almost no CO was released in the control sample (0 μM H_2O_2) (Fig. 1l). These results suggest that (Lo + FeCO)@MPDA@CAFM-PTP nanomedicine is stable and does not release CO in normal tissues, making it safe in a physiological environment.

3.3. *In vitro* safety, targeting, and anti-cancer effects of (Lo + FeCO)@MPDA@CAFM-PTP nanomedicine

We first evaluated the safety of MPDA and (Lo + FeCO)@MPDA@CAFM-PTP nanoparticles *in vitro*. Cytotoxicity tests for MPDA were performed on 3T3 cells and Panc-1 cells, which are representative of PC cells, while safety tests for (Lo + FeCO)@MPDA@CAFM-PTP were conducted on HUVEC cells, which are normal human endothelial cells. To enhance nanoparticle uptake by the cells, experiments were carried out in the dark, and the efficacy was evaluated using the CCK-8 assay. We found that both MPDA (Fig. 2a and b) and (Lo + FeCO)@MPDA@CAFM-PTP exhibited negligible cytotoxicity, even at a high concentration of 100 μg mL^{-1} (Fig. 2c). This suggests that MPDA is an excellent carrier with favorable biocompatibility, and that (Lo + FeCO)@MPDA@CAFM-PTP has no significant impact on normal cells.

The targeting ability of (Lo + FeCO)@MPDA@CAFM-PTP nanomedicine for PC was evaluated through a series of comparative experiments. In cell-based assays, we used a Transwell chamber to simulate the physiological conditions of PC as a solid tumor. TGF-β1-stimulated fibroblast (CAF) cells were seeded in the donor chamber to represent the ECM of PC, while PC (Panc-1) cells were seeded in the acceptor chamber (Fig. 2d). ICG labeled MPDA, (Lo + FeCO)@MPDA, (Lo + FeCO)@MPDA@CAFM, and (Lo + FeCO)@MPDA@CAFM-PTP were added to the donor chamber, respectively. After 12 hours of co-incubation, Panc-1 cells in the acceptor chamber were observed using a fluorescence microscope to detect intracellular fluorescence intensity and assess the targeting ability of the nanoparticles. The results showed that the strongest intracellular fluorescence signal in Panc-1 cells was observed in the (Lo + FeCO)@MPDA@CAFM-PTP-treated group, while almost no fluorescence signal was detected in the MPDA-treated group. Although both the (Lo + FeCO)@MPDA and (Lo + FeCO)@MPDA@CAFM-treated groups exhibited some intracellular fluorescence signals, the fluorescence intensity in the (Lo + FeCO)@MPDA@CAFM-treated group was significantly higher than that in the former (Fig. 2e). To further validate the active targeting function of PTP, Panc-1 cells were pre-incubated with a plectin-1 antibody before treatment with ICG-labeled (Lo + FeCO)@MPDA@CAFM-PTP nanoparticles. The results showed a marked reduction in the fluorescence signal in Panc-1 cells that had been blocked with plectin-1 antibody compared to the untreated cells. Since plectin-1 is the receptor for PTP, this finding indirectly confirms that the active targeting of (Lo + FeCO)@MPDA@CAFM-PTP nanomedicine is mediated by PTP (Fig. S5, ESI†).

The *in vitro* anti-cancer effect was assessed using a cellular live/dead assay. The results demonstrated that the (Lo + FeCO)@MPDA@CAFM-PTP-treated group exhibited the lowest Panc-1 cell viability compared to the other treatment groups. The cell viability in the MPDA-treated group showed no significant difference from the control group, indicating that MPDA had no cytotoxic effect on Panc-1 cells. The cell viability in the (Lo + FeCO)@MPDA@CAFM-treated group was higher than in the (Lo + FeCO)@MPDA@CAFM-PTP-treated group but still lower than in the (Lo + FeCO)@MPDA-treated group. Taken together, these findings confirm that (Lo + FeCO)@MPDA@CAFM-PTP nanomedicine exerts a potent cytotoxic effect on PC cells *in vitro* through its targeting ability (Fig. 2f).

To further investigate whether the cancer-killing effect induced by FeCO is mediated by CO rather than iron ions, we co-cultured Panc-1 cells with either FeCO or iron ions generated by the reaction between FeCO and H_2O_2. Cell viability was then measured using the CCK-8 assay. The results showed that the viability of Panc-1 cells treated with FeCO was significantly lower than that in the group treated with iron ions (Fig. S6, ESI†).

Previous studies have suggested that one mechanism underlying the anti-cancer effect of CO is the induction of intracellular secondary ROS bursts, which lead to cell apoptosis. We also detected intracellular ROS in Panc-1 cells by DCFH-DA, which is a specific probe for ROS detection. The results revealed that the (Lo + FeCO)@MPDA@CAFM-PTP treated group exhibited the highest ROS levels compared to all other groups, indicating significant intracellular oxidative stress (Fig. 2g).

3.4. *In vivo* targeting ability, anti-cancer effects, and safety of the (Lo + FeCO)@MPDA@CAFM-PTP nanomedicine

We then investigated the *in vivo* targeting ability, anti-cancer effects, and safety of the (Lo + FeCO)@MPDA@CAFM-PTP nanomedicine in subcutaneous tumor-bearing mice. To investigate the *in vivo* targeting ability of the nanomedicine, ICG-labeled MPDA, (Lo + FeCO)@MPDA, (Lo + FeCO)@MPDA@CAFM, and (Lo + FeCO)@MPDA@CAFM-PTP nanoparticles were injected into PC tumor-bearing mice *via* the tail vein.

Slight fluorescence signals were observed at the tumor site 2 hours after intravenous (I.V.) injection, with the fluorescence intensity gradually increasing over time and peaking at 24 hours post-injection. The (Lo + FeCO)@MPDA@CAFM-PTP treated group exhibited the strongest fluorescence intensity of ICG at the tumor sites compared to all other groups. In contrast, the MPDA-treated group showed only very weak fluorescence signals at the tumor rim. Both the (Lo + FeCO)@MPDA and (Lo + FeCO)@MPDA@CAF treated groups displayed noticeable fluorescence signals at the tumor sites, with the latter showing significantly higher fluorescence intensity (Fig. 3a). After 24 hours, the mice were sacrificed for *ex vivo* imaging, and the results were consistent with the *in vivo* imaging data (Fig. 3b). Additionally, we digested the organs and tumors with aqua regia and quantitatively

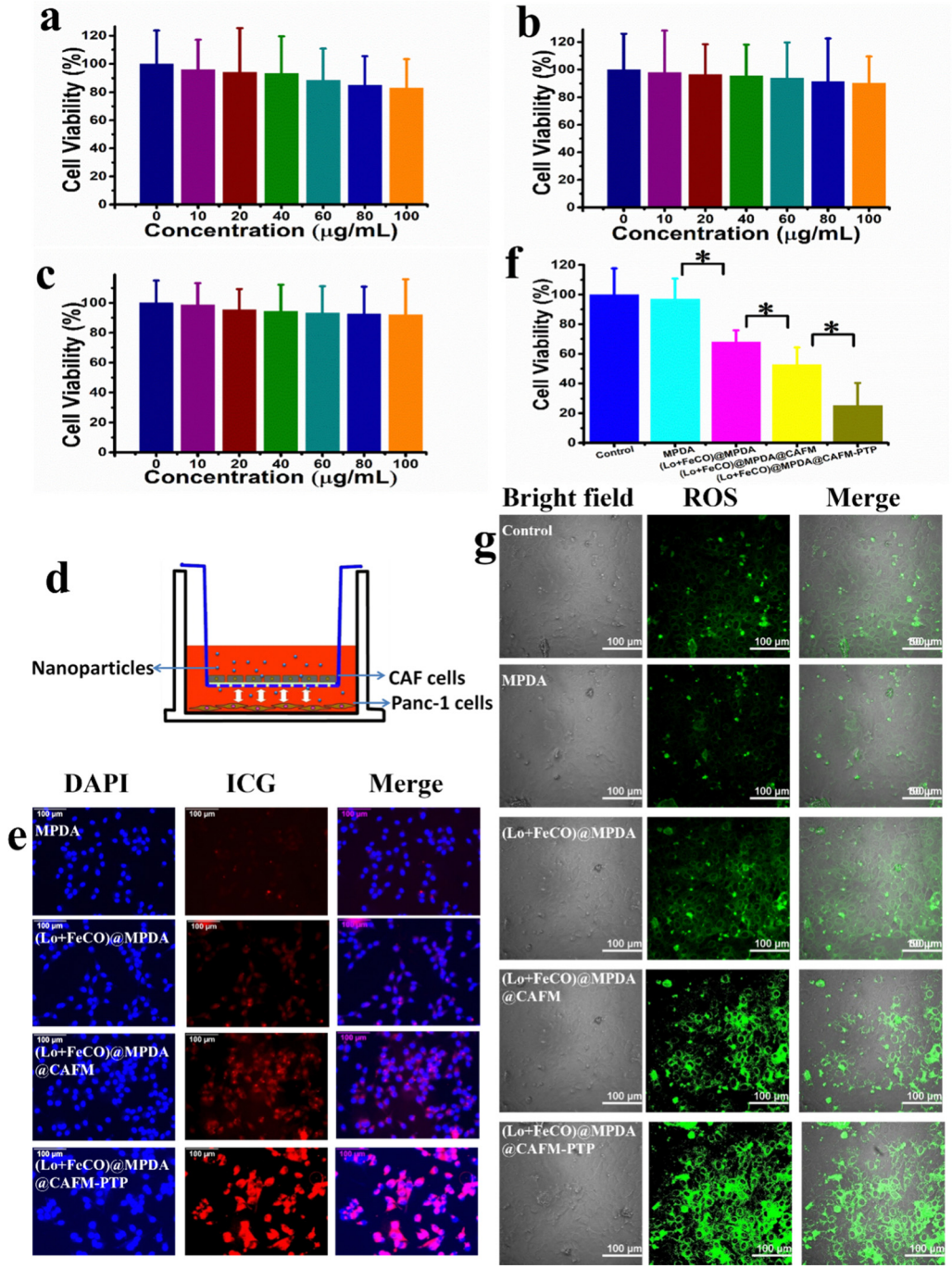

Fig. 2 Cytotoxicity of MPDA nanoparticles on Panc-1 cells (a) and 3T3 cells (b). (c) Cytotoxicity of (Lo + FeCO)@MPDA@CAFM-PTP nanomedicine on HUVEC cells. (d) Schematic illustration of the Transwell assay to simulate the physiological characteristics of PC as a solid tumor. (e) Fluorescence images of Panc-1 cells in the acceptor chamber of the Transwell after CAF cells in the donor chamber were treated with ICG-labeled MPDA, (Lo + FeCO)@MPDA, (Lo + FeCO)@MPDA@CAFM, and (Lo + FeCO)@MPDA@CAFM-PTP nanoparticles. (f) Anti-cancer effects on Panc-1 cells in the acceptor chamber of the Transwell after CAF cells in the donor chamber were treated with PBS, MPDA, (Lo + FeCO)@MPDA, (Lo + FeCO)@MPDA@CAFM, and (Lo + FeCO)@MPDA@CAFM-PTP nanoparticles. (g) Intracellular ROS images of Panc-1 cells in acceptor chamber of the Transwell after CAF cells in the donor chamber were treated with PBS, MPDA, (Lo + FeCO)@MPDA, (Lo + FeCO)@MPDA@CAFM, and (Lo + FeCO)@MPDA@CAFM-PTP nanoparticles. Data are presented as mean ± standard deviation (SD) (n = 6). Statistical significance is indicated by an asterisk (*$p < 0.05$).

analyzed the distribution of iron. The results revealed the highest iron content in the tumor tissue of the (Lo + FeCO)@MPDA@CAF treated group, which closely aligned with the fluorescence imaging results (Fig. 3c).

We further performed co-localization of the immunofluorescence signals for plectin-1 with the ICG fluorescence signals of nanoparticles to assess the targeting ability of (Lo + FeCO)@MPDA@CAFM-PTP in tumor slices. The results showed

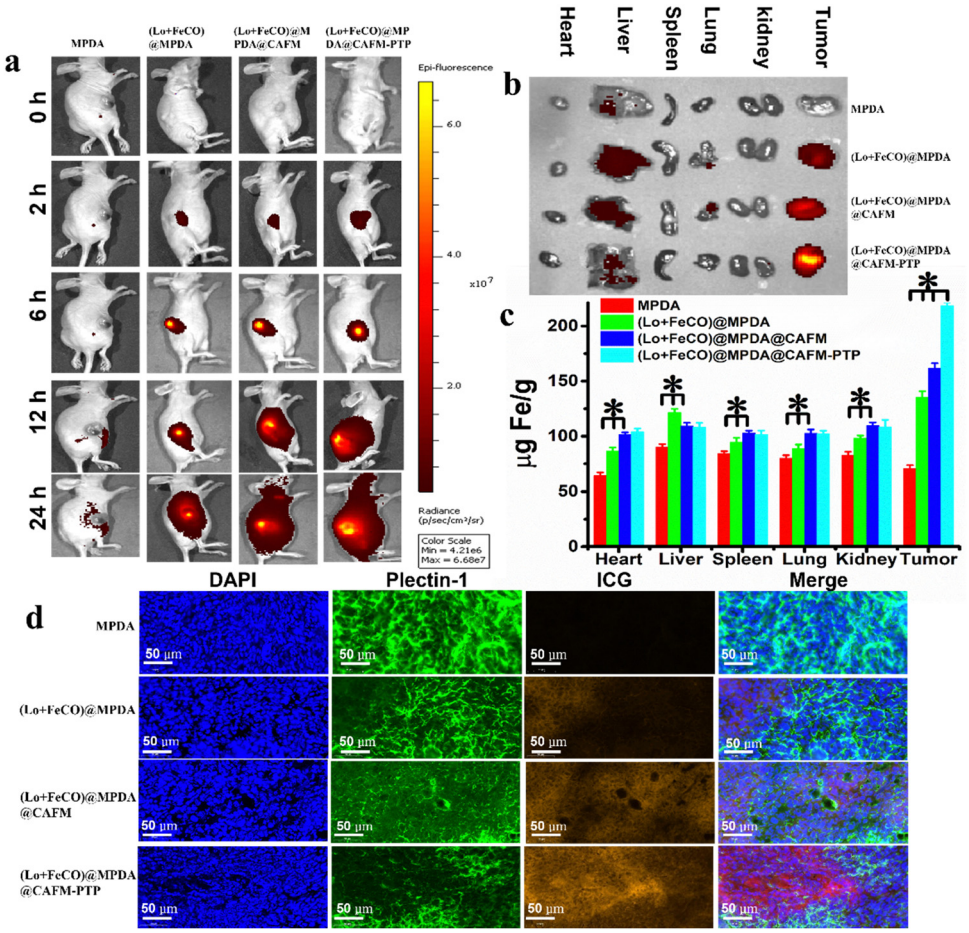

Fig. 3 *In vivo* targeting ability of (Lo + FeCO)@MPDA@CAFM-PTP nanomedicine in living mice. (a) *In vivo* fluorescence images of PC tumor-bearing mice at various time points after intravenous injection of ICG-labeled MPDA, (Lo + FeCO)@MPDA, (Lo + FeCO)@MPDA@CAFM, and (Lo + FeCO)@MPDA@CAFM-PTP nanoparticles. (b) *Ex vivo* fluorescence images of major organs and tumors harvested from mice 24 hours after injection. (c) Quantitative analysis of Fe content in major organs and tumors following nanoparticle injection, determined using ICP-OES. (d) Fluorescence images showing co-localization of tumor slices to assess the distribution of nanoparticles and plectin-1 expression in different groups. Data are presented as mean ± standard deviation (SD) (n = 3). Statistical significance in Fe content between the different treatment groups is indicated by an asterisk ($*p < 0.05$).

that the ICG fluorescence signals of the nanoparticles coincided with the immunofluorescence signals of plectin-1. Notably, the (Lo + FeCO)@MPDA@CAFM-PTP-treated group exhibited the strongest ICG fluorescence intensity in the tumor slices compared to all other groups, which was consistent with the *in vivo* and *ex vivo* imaging results (Fig. 3d).

These results indicate that the (Lo + FeCO)@MPDA@CAFM-PTP nanomedicine can effectively penetrate the ECM and bind to PC cells due to cell membrane homologous adhesion, ECM disruption, and plectin-1 targeting. This is consistent with our design and demonstrates that (Lo + FeCO)@MPDA@CAFM-PTP exhibits excellent targeting ability toward PC.

Given the *in vitro* and *in vivo* targeting ability and the observed *in vitro* anti-cancer effects of the (Lo + FeCO)@MPDA@CAFM-PTP nanomedicine, we further investigated its *in vivo* anti-cancer efficacy in the PC tumor-bearing mouse model. The experimental protocol involved randomly dividing the PC tumor-bearing mice into five groups (n = 5). These groups were intravenously injected *via* tail vein with PBS (control), MPDA, (Lo + FeCO)@MPDA, (Lo + FeCO)@MPDA@CAFM, or (Lo + FeCO)@MPDA@CAFM-PTP nanoparticles. Following the treatment, we collected blood, major organs and tumors for evaluation of biosafety and therapeutic effectiveness (Fig. 4a).

We evaluated the biosafety of (Lo + FeCO)@MPDA@CAFM-PTP nanomedicine through blood biochemical analysis, H&E staining of major organ slices, and body weight measurement. Serum biochemical parameters (including ALT, AST, TBIL, CR, and BUN) showed no significant damage to hepatic or renal functions in the nanomedicine-treated groups compared to the control group (Fig. S7a–e, ESI†). Furthermore, there were no significant differences in hematological parameters such as white blood cells (WBC), red blood cells (RBC), hemoglobin (HGB), and platelet (PLT) between the PBS control and the nanomedicine-treated groups (Table S2, ESI†). The structure and morphology of major organs were assessed using H&E

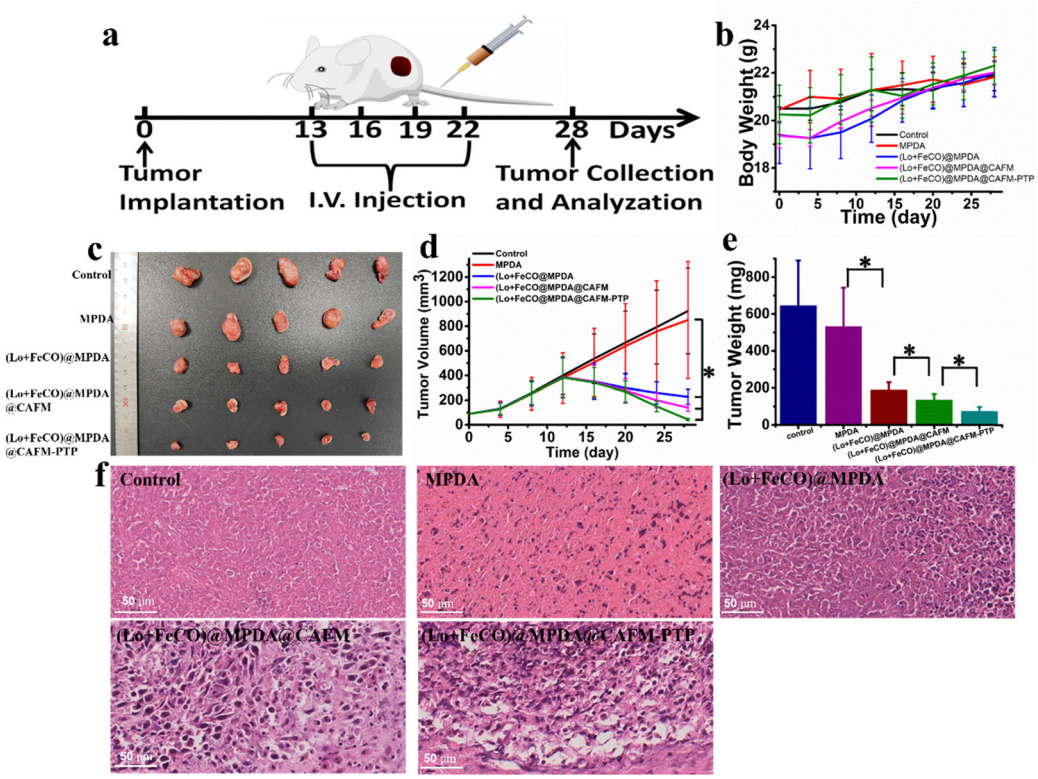

Fig. 4 (a) Schematic illustration of the treatment workflow in PC tumor-bearing mice. (b) Changes in body weight of mice throughout the treatment period. (c) Images of excised PC tumors after treatment with different drug formulations. (d) Tumor growth curves during the course of treatment. (e) Average tumor weights for each treatment group. (f) Histological analysis of tumor sections stained with H&E after different treatments. Data are presented as mean ± standard deviation (SD) (n = 5). Statistical significance is indicated by an asterisk (*$p < 0.05$).

staining. The results indicated that, compared to the control group, the treatment groups caused no noticeable damage to major organs, including the heart, liver, spleen, lungs, and kidneys (Fig. S8a–e, ESI†). Additionally, no significant loss in body weight was observed in mice during the course of the experiment (Fig. 4b). These findings suggest that (Lo + FeCO)@MPDA@CAFM-PTP nanomedicine demonstrates good biocompatibility and biosafety *in vivo*.

To evaluate the *in vivo* anti-cancer efficacy of (Lo + FeCO)@MPDA@CAFM-PTP nanomedicine, tumor volume and weight were measured. The results indicated that tumor growth in the MPDA-treated group was similar to that in the PBS control group, suggesting that MPDA nanoparticles did not exhibit anti-cancer effects *in vivo*. In contrast, all drug-loaded groups showed varying degrees of tumor growth inhibition. The (Lo + FeCO)@MPDA treatment slightly suppressed tumor growth, while the (Lo + FeCO)@MPDA@CAFM treatment enhanced the anti-cancer effect to a certain extent due to its CAF cell membrane-mediated homologous adhesion. Notably, among all the treated groups, the (Lo + FeCO)@MPDA@CAFM-PTP nanomedicine exhibited the most effective anti-cancer effect, nearly achieving complete tumor growth inhibition due to its excellent targeting ability (Fig. 4c–e). Further analysis of peritumor lymph nodes revealed that the number and mean volume of peritumor lymph nodes in the (Lo + FeCO)@MPDA@CAFM-PTP treatment group were significantly smaller than in any other group, further supporting the conclusion that (Lo + FeCO)@MPDA@CAFM-PTP nanomedicine provides effective anti-cancer therapy (Fig. S9a and b, ESI†).

H&E staining of tumor slices was further conducted to assess the anti-cancer effect of (Lo + FeCO)@MPDA@CAFM-PTP nanomedicine. The results showed no significant cell necrosis in the PBS control and MPDA-treated groups. In contrast, increased cell necrosis was observed in the (Lo + FeCO)@MPDA@CAFM-PTP-treated group compared to the (Lo + FeCO)@MPDA and (Lo + FeCO)@MPDA@CAFM groups (Fig. 4f).

TUNEL staining was also performed to detect cell apoptosis in tumor sections. The results demonstrated that the most significant apoptosis was induced in the (Lo + FeCO)@MPDA@CAFM-PTP treatment group compared to the (Lo + FeCO)@MPDA and (Lo + FeCO)@MPDA@CAFM groups. Overall, these analyses indicated that (Lo + FeCO)@MPDA@CAFM-PTP outperformed both (Lo + FeCO)@MPDA and (Lo + FeCO)@MPDA@CAFM in the treatment of PC (Fig. 5).

Since the release of CO from FeCO is triggered by the overproduction of intracellular ROS in tumor cells, and the anti-cancer effect of CO is mediated by the ROS burst, we conducted an oxidative stress assay on tumor slices using immunohistofluorescence staining to detect ROS. The results revealed clear immunohistofluorescence signals for ROS in both the control and MPDA-treated groups. However, the ROS signals were significantly stronger in the (Lo + FeCO)@MPDA,

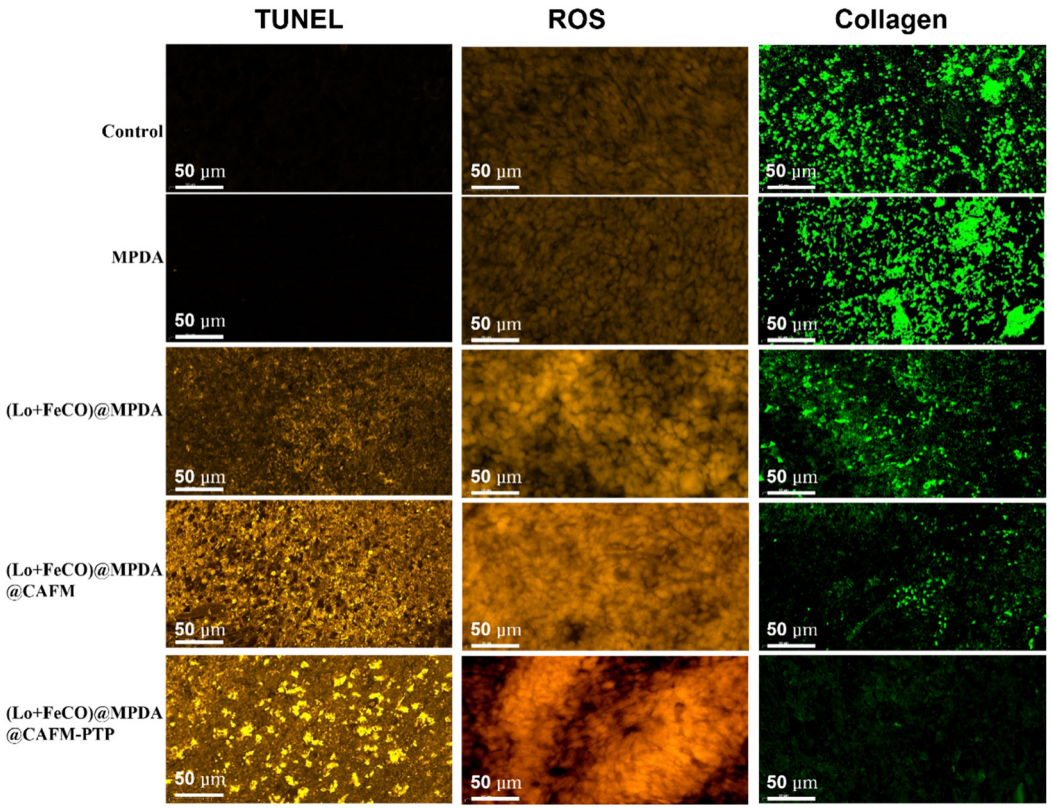

Fig. 5 Immunohistofluorescence staining of TUNEL, ROS and collagen of tumor slices from different treatment groups.

(Lo + FeCO)@MPDA@CAFM, and (Lo + FeCO)@MPDA@CAFM-PTP-treated groups. Notably, the (Lo + FeCO)@MPDA@CAFM-PTP treatment group exhibited the most intense ROS immunohistofluorescence signals, which was consistent with the *in vitro* oxidative stress analysis results (Fig. 5).

To investigate the matrix degradation effect of (Lo + FeCO)@MPDA@CAFM-PTP nanomedicine on the ECM of PC *in vivo*, we performed immunofluorescence staining for collagen, the primary component of the tumor matrix. In both the PBS control group and the MPDA-treated group, abundant collagen fibers were observed in the tumor tissue. In contrast, treatment with Lo-loaded formulations, particularly (Lo + FeCO)@MPDA@CAFM and (Lo + FeCO)@MPDA@CAFM-PTP, resulted in significant matrix degradation, as evidenced by decreased collagen signals due to CAF cell membrane homologous adhesion and Lo release. Interestingly, matrix degradation in the (Lo + FeCO)@MPDA@CAFM group was slightly less pronounced compared to the (Lo + FeCO)@MPDA@CAFM-PTP group, possibly due to the enhanced retention ability of (Lo + FeCO)@MPDA@CAFM-PTP through active targeting, which facilitated a more substantial release of Lo (Fig. 5). We also analyzed the expression of α-SMA, a characteristic marker of fibrosis, and the results were consistent with those from the collagen immunofluorescence staining assay (Fig. S10a–e, ESI†). Furthermore, we conducted an extracellular matrix assay using tumor histopathological slices following treatment with different drug formulations, and the results aligned with the collagen and α-SMA immunofluorescence findings (Fig. S11, ESI†). These results suggest that the (Lo + FeCO)@MPDA@CAFM-PTP nanomedicine effectively degrades the ECM in PC. The *in vitro* and *in vivo* studies demonstrated that we have designed a nanomedicine capable of effectively targeting PC, overcoming delivery barriers, and achieving a satisfactory treatment outcome.

4. Discussion

PC is characterised by high lethality, rapid progression, extremely poor prognosis, and limited treatment efficacy.[1,6,8] It has the worst prognosis among all solid tumors, with a 5-year overall survival rate for patients with advanced PC of less than 5%, and a median survival time of less than one year.[5,7,40,46] Once the disease reaches the metastatic stage, the 5-year survival rate drops to below 3%.[47] The grim prognosis of PC is largely due to the lack of specific symptoms, early metastasis, complex tumor biology, and a dense, heterogenous microenvironment known as the stroma.[6] To better simulate the physiological characteristics of PC, we utilized a Transwell assay *in vitro* and a mixture of Panc-1 and 3T3 cells *in vivo*.

Because fewer than 30% of PC cases are eligible for surgical resection, chemotherapy remains the first-line treatment. However, the use of highly toxic chemotherapeutic drugs often exposes patients to serious side effects, causing significant

pain, psychological burden, and a reduced quality of life.[1,5,9] In recent years, unique gas-generating nanoplatforms have emerged as an efficient therapeutic strategy.[10] Notably, among all gas transmitters, CO demonstrates one of the most potent antitumor effects, effectively inhibiting tumor proliferation and metastasis. CO also plays an anti-apoptotic role in normal cells, maintaining a delicate balance between cytoprotection and cytotoxicity.[9–11,14] Additionally, CO can induce tumor vascular dilatation, enhance the EPR effect, and promote the accumulation of nanomedicines in tumor tissues.[15,16]

Since CO is also known to be a toxic gas, targeted delivery and controlled release of CO are crucial strategies for enhancing its therapeutic efficacy while minimizing side effects.[9] Smart nanoplatforms capable of integrating with CORMs may address the challenges of controlling CO release and ensuring target selectivity in CO-based therapies.[13] In this study, we use the CORM molecule FeCO as a CO source. Once the nanomedicine is internalized by PC cells, FeCO reacts with the intracellularly enriched ROS, undergoing a Fenton-like reaction to release CO gas locally. This process leads to tumor inhibition without causing significant side effects.[9,11,12,15]

Although the exact mechanism behind CO's anticancer efficacy remains unclear, its action on mitochondria and subsequent dysfunction may be a key factor.[11,12,14] Mitochondrial dysfunction can significantly impair ATP synthesis, which is essential for DNA repair, and increase the expression of pro-apoptotic molecules, ultimately leading to tumor cell apoptosis.[12,14] Additionally, damage to the mitochondrial respiratory chain can result in the production of excessive ROS, which can affect cell viability.[10–12,14] In this study, elevated ROS levels were observed in the nanomedicine treatment groups both *in vitro* and *in vivo*.

Although nanomedicine's active targeting ability can improve treatment efficacy to some extent, the stroma within the TME in PC remains a significant barrier to effective drug delivery.[39] Previous studies have demonstrated that Lo can downregulate collagen in the TME, thereby enhancing the deep penetration of nanoparticles into solid tumors.[15,25] By combining Lo and FeCO into a single nanoplatform, it is possible to not only reduce the PC matrix barrier but also leverage the potent antitumor effects of CO.[26] The results of this study revealed that both collagen and α-SMA were significantly reduced in the (Lo + FeCO)@MPDA@CAFM-PTP nanomedicine-treated group, consistent with previous studies.[12,48] The primary mechanism behind Lo's antifibrotic effects is likely its ability to inactivate CAF cells, thereby decreasing ECM production and reducing CAF cell density.[24,25,47,49]

The most important prerequisite for the application of nanoplatform is biosafety.[50] In this study, we selected MPDA nanoparticles as the drug carrier because dopamine is a natural hormone in the human body.[36] Previous studies have demonstrated that MPDA does not induce long-term toxicity, even at high median lethal dose, due to its excellent biocompatibility and biodegradability.[43,50,51] The degradation products of MPDA are monomers and oligomers, none of which have pharmacological effects similar to dopamine.[28] So far, MPDA has shown exceptional biosafety in most preclinical experiments. In this study, we confirmed MPDA's biosafety both *in vitro* and *in vivo*, with results indicating excellent biocompatibility.

The TME of PC is more acidic (pHe 6.2–7.0) than that of healthy tissues, primarily due to hypoxia and the Warburg effect. This acidity can be exploited in the design of nanoplatforms that respond to changes in pH for targeted drug delivery.[22,23,48] Another key reason we selected MPDA as the controlled-release drug carrier is its strong sensitivity to pH. It remains stable under normal physiological conditions but degrades easily in the acidic microenvironment of cancer cells, allowing for drug release at the target site.[17,29,44]

Due to the exogenous nature of (Lo + FeCO)@MPDA nanoparticles, we coated them with CAFM nanovesicles for biomimetic purposes. Coating nanoparticles with cell membranes helps retain many desirable functions that are difficult to achieve through chemical synthesis, such as immune evasion and homologous adhesion.[27] In this study, the primary reason for coating the nanoparticles with CAFM nanovesicles was to enable homologous adhesion. When nanoparticles are coated with a cell membrane, the nanoformulation shares the same cell adhesion molecules as the source cells, allowing for source cell-specific targeting through the homologous binding mechanism.[27,39] CAF cells, or stromal fibroblasts, are the most abundant stromal cells in the TME of PC, producing large amounts of collagen, hyaluronic acid, and other ECM components.[1,52] Through the homologous mechanism, (Lo + FeCO)@MPDA@CAFM-PTP nanomedicine can selectively target CAF cells in PC tissue, leading to increased drug accumulation in the tumor.[39]

Since most of the tumor cells in PC tissue are surrounded by the ECM, active targeting of tumor cells is crucial. Carbohydrate antigen 19-9 (CA19-9) is the only serum biomarker currently used for PC diagnosis, but its sensitivity and specificity are low, as many benign pancreatic diseases can also result in elevated CA19-9 levels.[7,40,53,54] Plectin-1 is aberrantly expressed on the surface of PC cells, and recent studies suggest it could serve as a novel biomarker for PC.[7,41] In this study, we enhanced the active targeting ability of (Lo + FeCO)@MPDA@CAFM by conjugating them with the targeting molecule PTP, which can specifically recognize and bind to plectin-1.

5. Limitations

To uphold ethical standards and ensure animal welfare, we limited the progression of PC tumor-bearing mice, preventing them from reaching cachexia or succumbing to cancer. As a result, survival curve analysis was not performed in this study. Additionally, long-term outcomes such as tumor recurrence and metastasis after treatment were not investigated. Future studies with extended follow-up periods and survival assessments will be essential to fully evaluate the long-term therapeutic potential of this nanomedicine.

6. Conclusions

In conclusion, this study successfully developed the (Lo + FeCO)@MPDA@CAFM-PTP nanomedicine, which effectively

targets PC tumors, degrades the tumor matrix, and kills cancer cells. These effects can be attributed to CAF cell membrane-homologous adhesion, plectin-1 recognition, Lo matrix degradation, and the inhibitory effect of CO on cancer cells. The results demonstrated that the targeting ability and anti-cancer effects of the (Lo + FeCO)@MPDA@CAFM-PTP nanomedicine were significantly stronger than those of other nanoformulations. This nanomedicine holds promise as a potential strategy for the treatment of other solid tumors.

Author contributions

The manuscript was written through contributions of all authors. All authors have given approval to the final version of the manuscript.

Data availability

The data supporting this article have been included as part of the ESI.†

Conflicts of interest

The authors declare no competing financial interest.

Acknowledgements

The authors thank the Editor and three anonymous reviewers for their insightful comments and suggestions. The authors sincerely appreciate the funding support from the National Natural Science Foundation of China (82372968), Medical Engineering Joint Fund of Fudan University (XM03231533).

References

1 H. Song and C. Jiang, *Expert Opin. Drug Delivery*, 2022, **19**, 281–301.
2 X. Tao, V. L. Go and G. G. N. Xiao, *Acta Physiol. Sin.*, 2021, **73**, 197–207.
3 L. Zhang, J. Li, L. Zong, X. Chen, K. Chen, Z. Jiang, L. Nan, X. Li, W. Li, T. Shan, Q. Ma and Z. Ma, *Oxid. Med. Cell. Longevity*, 2016, **2016**, 1616781.
4 A. Banstola, T. T. Pham, J. H. Jeong and S. Yook, *Drug Deliv.*, 2019, **26**, 629–640.
5 Q. Wang, X. Zhu, Z. Wu, T. Sun, W. Huang, Z. Wang, X. Ding, C. Jiang and F. Li, *J. Mater. Chem. B*, 2020, **8**, 2410–2417.
6 A. B. Popov, F. Melle, E. Linnane, C. Gonzalez-Lopez, I. Ahmed, B. Parshad, C. O. Franck, H. Rahmoune, F. M. Richards, D. Munoz-Espin, D. I. Jodrell, D. Fairen-Jimenez and L. Fruk, *Nanoscale*, 2022, **14**, 6656–6669.
7 K. A. Kelly, N. Bardeesy, R. Anbazhagan, S. Gurumurthy, J. Berger, H. Alencar, R. A. Depinho, U. Mahmood and R. Weissleder, *PLoS Med.*, 2008, **5**, e85.
8 W. Li, L. Cao, X. Chen, J. Lei and Q. Ma, *Oncol. Rep.*, 2016, **35**, 1718–1726.
9 J. Meng, Z. Jin, P. Zhao, B. Zhao, M. Fan and Q. He, *Sci. Adv.*, 2020, **6**, eaba1362.
10 X. Yao, P. Yang, Z. Jin, Q. Jiang, R. Guo, R. Xie, Q. He and W. Yang, *Biomaterials*, 2019, **197**, 268–283.
11 D. Wu, X. Duan, Q. Guan, J. Liu, X. Yang, F. Zhang, P. Huang, J. Shen, X. Shuai and Z. Cao, *Adv. Funct. Mater.*, 2019, 29.
12 B. Zhao, P. Zhao, Z. Jin, M. Fan, J. Meng and Q. He, *J. Nanobiotechnol.*, 2019, **17**, 75.
13 Z. Yuan, C. Lin, L. Dai, Y. He, J. Hu, K. Xu, B. Tao, P. Liu and K. Cai, *Small*, 2021, **17**, e2007522.
14 Y. Li, J. Dang, Q. Liang and L. Yin, *ACS Cent. Sci.*, 2019, **5**, 1044–1058.
15 H. Yao, K. Xu, J. Zhou, L. Zhou and S. Wei, *ACS Biomater. Sci. Eng.*, 2020, **6**, 450–462.
16 Y. Sun, C. An, L. Wu, W. Zeng, J. Wang, Y. Wang, J. He, G. Gao and D. Ye, *ACS Nano*, 2021, **15**, 16298–16313.
17 X. Li, C. Xie, H. Xia and Z. Wang, *Langmuir*, 2018, **34**, 9974–9981.
18 Y. Zhu, M. Deng, N. Xu, Y. Xie and X. Zhang, *Front. Chem.*, 2021, **9**, 650899.
19 E. C. Cheung, G. M. DeNicola, C. Nixon, K. Blyth, C. F. Labuschagne, D. A. Tuveson and K. H. Vousden, *Cancer Cell*, 2020, **37**, 168–182.
20 N. Abdel Hadi, G. Reyes-Castellanos and A. Carrier, *Int. J. Mol. Sci.*, 2021, **22**, 1534.
21 T. Huo, X. Zhang, M. Qian, H. Nie, D. Liang, C. Lin, Y. Yang, W. Guo, U. Lachelt and R. Huang, *Adv. Sci.*, 2022, **9**, e2200608.
22 X. Han, Y. Xu, M. Geranpayehvaghei, G. J. Anderson, Y. Li and G. Nie, *Biomaterials*, 2020, **232**, 119745.
23 X. Han, Y. Li, Y. Xu, X. Zhao, Y. Zhang, X. Yang, Y. Wang, R. Zhao, G. J. Anderson, Y. Zhao and G. Nie, *Nat. Commun.*, 2018, **9**, 3390.
24 V. P. Chauhan, J. D. Martin, H. Liu, D. A. Lacorre, S. R. Jain, S. V. Kozin, T. Stylianopoulos, A. S. Mousa, X. Han, P. Adstamongkonkul, Z. Popovic, P. Huang, M. G. Bawendi, Y. Boucher and R. K. Jain, *Nat. Commun.*, 2013, **4**, 2516.
25 B. Diop-Frimpong, V. P. Chauhan, S. Krane, Y. Boucher and R. K. Jain, *Proc. Natl. Acad. Sci. U. S. A.*, 2011, **108**, 2909–2914.
26 X. Y. Yang, J. G. Zhang, Q. M. Zhou, J. N. Yu, Y. F. Lu, X. J. Wang, J. P. Zhou, X. F. Ding, Y. Z. Du and R. S. Yu, *J. Nanobiotechnol.*, 2022, **20**, 524.
27 R. H. Fang, C. M. Hu, B. T. Luk, W. Gao, J. A. Copp, Y. Tai, D. E. O'Connor and L. Zhang, *Nano Lett.*, 2014, **14**, 2181–2188.
28 T. Chen, B. Zhuang, Y. Huang, Y. Liu, B. Yuan, W. Wang, T. Yuan, L. Du and Y. Jin, *Acta Pharm. Sin. B*, 2022, **12**, 2522–2532.
29 L. Dai, D. Wei, J. Zhang, T. Shen, Y. Zhao, J. Liang, W. Ma, L. Zhang, Q. Liu and Y. Zheng, *Cell Proliferation*, 2021, **54**, e13130.
30 M. Ding, Z. Miao, F. Zhang, J. Liu, X. Shuai, Z. Zha and Z. Cao, *Biomater. Sci.*, 2020, **8**, 4157–4165.

31 J. Yang, W. Zeng, X. Fu, L. Chen, X. Yu, P. Xu, W. Huang, F. Leng, C. Yu and Z. Yang, *J. Mater. Chem. B*, 2022, **10**, 5644–5654.
32 X. Hu, Y. Lu, X. Shi, T. Yao, C. Dong and S. Shi, *Chem. Commun.*, 2019, **55**, 14785–14788.
33 Y. C. Wang, H. L. Dai, Z. H. Li, Z. Y. Meng, Y. Xiao and Z. Zhao, *J. Mater. Chem. B*, 2021, **9**, 7401–7408.
34 H. Peng, D. Wang, D. Ma, Y. Zhou, J. Zhang, Y. Kang and Q. Yue, *ACS Appl. Mater. Interfaces*, 2022, **14**, 23888–23895.
35 Z. Wang, J. Zhang, F. Chen and K. Cai, *Analyst*, 2017, **142**, 2796–2804.
36 D. Ren, G. R. Williams, Y. Zhang, R. Ren, J. Lou and L. M. Zhu, *ACS Appl. Bio Mater.*, 2022, **5**, 123–133.
37 S. Li, Y. Gan, C. Lin, K. Lin, P. Hu, L. Liu, S. Yu, S. Zhao and J. Shi, *ACS Appl. Bio Mater.*, 2021, **4**, 1605–1615.
38 Y. Wang, W. Ge, Z. Ma, G. Ji, M. Wang, G. Zhou and X. Wang, *APL Bioeng.*, 2022, **6**, 026101.
39 J. Li, X. Zhen, Y. Lyu, Y. Jiang, J. Huang and K. Pu, *ACS Nano*, 2018, **12**, 8520–8530.
40 D. Bausch, S. Thomas, M. Mino-Kenudson, C. C. Fernandez-del, T. W. Bauer, M. Williams, A. L. Warshaw, S. P. Thayer and K. A. Kelly, *Clin. Cancer Res.*, 2011, **17**, 302–309.
41 B. G. Song, W. Kwon, H. Kim, E. M. Lee, Y. M. Han, H. Kim, Y. Byun, K. B. Lee, K. H. Lee, K. T. Lee, J. K. Lee, J. Y. Jang and J. K. Park, *Front. Oncol.*, 2020, **10**, 616440.
42 H. Pawar, M. K. Kashyap, N. A. Sahasrabuddhe, S. Renuse, H. C. Harsha, P. Kumar, J. Sharma, K. Kandasamy, A. Marimuthu, B. Nair, S. Rajagopalan, J. Maharudraiah, C. S. Premalatha, K. V. Kumar, M. Vijayakumar, R. Chaerkady, T. S. Prasad, R. V. Kumar, R. V. Kumar and A. Pandey, *Cancer Biol. Ther.*, 2011, **12**, 510–522.
43 M. Yang, N. Zhang, T. Zhang, X. Yin and J. Shen, *Drug Deliv.*, 2020, **27**, 367–377.
44 M. Shao, C. Chang, Z. Liu, K. Chen, Y. Zhou, G. Zheng, Z. Huang, H. Xu, P. Xu and B. Lu, *Colloids Surf., B*, 2019, **183**, 110427.
45 H. Suo, M. Li, R. Liu and L. Xu, *Colloids Surf., B*, 2021, **206**, 111960.
46 Y. Li, Z. Zhao, H. Liu, J. P. Fetse, A. Jain, C. Y. Lin and K. Cheng, *ACS Appl. Mater. Interfaces*, 2019, **11**, 45390–45403.
47 A. Kasi, J. Allen, K. Mehta, P. Dandawate, S. Saha, S. Bossmann, S. Anant and W. Sun, *J. Clin. Transl. Res.*, 2021, **7**, 257–262.
48 B. Wu, Z. Sun, J. Wu, J. Ruan, P. Zhao, K. Liu, C. X. Zhao, J. Sheng, T. Liang and D. Chen, *Angew. Chem., Int. Ed.*, 2021, **60**, 9284–9289.
49 A. Hauge and E. K. Rofstad, *J. Transl. Med.*, 2020, **18**, 207.
50 M. Zhang, H. Du, Y. Guan, J. Liu, S. Wang, H. Li, W. Zhang, H. Han, M. Zhang and L. Chen, *Front. Bioeng. Biotechnol.*, 2022, **10**, 927348.
51 X. Li, Z. Wei, L. Wu, H. Lv, Y. Zhang, J. Li, H. Yao, H. Zhang, B. Yang, X. Xu and J. Jiang, *Biomater. Sci.*, 2020, **8**, 5362–5375.
52 H. Shao, M. Moller, D. Wang, A. Ting, M. Boulina and Z. J. Liu, *J. Visualized Exp.*, 2020, **156**, e60660.
53 Q. Dong, X. Jia, Y. Wang, H. Wang, Q. Liu, D. Li, J. Wang and E. Wang, *J. Nanobiotechnol.*, 2022, **20**, 94.
54 T. D. Li, R. Zhang, H. Chen, Z. P. Huang, X. Ye, H. Wang, A. M. Deng and J. L. Kong, *Chem. Sci.*, 2018, **9**, 5372–5382.